Journal of Solid State Chemistry **161,** 348–354 (2001)
doi:10.1006/jssc.2001.9334, available online at http://www.idealibrary.com on IDEAL®

Order–Disorder Transition in $(Cu_{0.5}Cr_{0.5})Sr_2CuO_x$ under High-Pressure and High-Temperature Conditions

T. Drezen,* S. M. Loureiro,*,[1] T. Nagai,*,† T. Asaka,* Y. Matsui,* A. Yamazaki,† and E. Takayama-Muromachi*,[2]

*National Institute for Research in Inorganic Materials, 1-1 Namiki, Tsukuba, Ibaraki 305-0044, Japan; and †Department of Resources and Environmental Engineering, School of Science and Engineering, Waseda University, 3-4-1 Ohkubo, Shinjuku, Tokyo 169-8555, Japan

Received February 7, 2001; revised July 17, 2001; accepted August 1, 2001

The $(Cu_{0.5}Cr_{0.5})Sr_2CuO_x$ phase is the first member of the $(Cu_{0.5}Cr_{0.5})Sr_2Ca_{n-1}Cu_nO_{2n+3}$ homologous series, having a layered structure with a single CuO_2 plane. Numerous samples of this system were prepared under high-pressure/high-temperature conditions while varying the x value. The phases crystallize with tetragonal symmetry when the samples are quenched to room temperature, while they show orthorhombic symmetry when slow cooled (with the exception of the $x = 5.0$ sample). Transmission electron microscopic data collected on several samples have allowed us to suggest that the origin of the orthorhombic distortion in the slowly cooled phases lies in the ordered arrangement of copper, chromium, and oxygen atoms in the $(Cu_{0.5}Cr_{0.5})$ plane. We have also concluded on the absence of superconductivity in the (Cu, Cr)-1201 phases. © 2001 Academic Press

Key Words: **(Cu, Cr)-1201; high-pressure synthesis; order–disorder transition; X-ray powder diffraction; HRTEM.**

INTRODUCTION

Recently, a new superconducting homologous series with general formula $(Cu, Cr)Sr_2Ca_{n-1}Cu_nO_{2n+3}$ ((Cu, Cr)-12$(n-1)n$) was discovered under high pressure (1). This system presents the widest range of synthesized members as bulk materials from $n = 1$ to $n = 9$. Among them, the $n = 2$–7 members show superconductivity with the highest T_c of 103 K ($n = 3$). A wide range of doping states of holes, from nonsuperconducting overdoped (for $n = 1$) to nonsuperconducting underdoped (for $n \geq 8$) via the optimum doping level at $n = 3$, was suggested. Although the exact structural features have not been elucidated yet, there may be different types of chromium coordination throughout the series, and even within the same member of the series.

The first member of the series $(Cu_{0.5}Cr_{0.5})Sr_2CuO_{5+\delta}$ ((Cu, Cr)-1201) has the simplest structure with a single CuO_2 plane per unit cell and can accommodate a large amount of excess oxygen. In the previously reported (Cu, Cr)-1201 sample, the excess oxygen content was estimated to be $\delta \approx 0.3$, and the average copper valence to be $\approx 2.8+$, taking into account the presence of the copper vacancies in the (Cu, Cr) plane (1). This suggested that superconductivity might be induced by decreasing the excess oxygen content. In the present study, we varied its oxygen content in order to induce superconductivity. However, no bulk superconductivity was observed in the (Cu, Cr)-1201 samples but a weak superconducting signal was sometimes observed due to a higher-order member of the analogous $(Cu, Cr)Sr_2Sr_{n-1}Cu_nO_{2n+3}$ family with $n > 1$ included as an impurity phase.

We found instead that, depending on the excess oxygen content and the synthesis conditions, the (Cu, Cr)-1201 phase crystallizes with two different symmetries, tetragonal and orthorhombic. In this study, we propose a mechanism of the tetragonal-to-orthorhombic transition based on X-ray diffraction and high-resolution transmission electron microscopy (HRTEM) studies. DC magnetic susceptibilities and DC electric conductivities of the (Cu, Cr)-1201 phases are also presented.

EXPERIMENTAL

Cr_2O_3 (99.9%), $SrCuO_2$, SrO_2, and CuO (99.9%) were used to prepare nominal mixtures of $(Cu_{0.5}Cr_{0.5})Sr_2CuO_x$ ($5.0 \leq x \leq 5.7$). $SrCuO_2$ was prepared through solid state reaction of CuO and $SrCO_3$ (99.9%) at 1000°C for 6 days. SrO_2 was synthesized through a solution route previously described (2). About 300 mg of the initial mixture was sealed in gold capsules and allowed to react in a belt-type high-pressure apparatus at 6 GPa and 1250°C. The samples were heated for 2 h, and subsequently quenched or slowly cooled to room temperature while keeping the pressure constant at

[1]Present address: Department of Chemistry, Princeton University, Princeton, NJ 08544.

[2]To whom correspondence should be addressed. Fax: 81-298-58-5650. E-mail: muromachi.eiji@nims.go.jp

0022-4596/01 $35.00

6 GPa. In the quenching procedure, the heating electric current was shut off instantaneously. A very large quenching rate is expected in this process because a large mass of the high-pressure apparatus works as a huge heat sink. In the slow-cooling procedure, the temperature was linearly decreased with time to room temperature over 3 h. To check possible oxygen loss, the gold capsules were carefully weighed before and after the high-pressure run. We rejected results with weight losses larger than 0.2 mg for a total weight (powder + capsule) of $\approx$1.1 g.

X-ray powder diffraction patterns were collected by a powder diffractometer (Phillips PW1800) in the Bragg-Brentano geometry. Cu$K\alpha$ radiation (40 kV, 50 mA), a 0.02 step size, and 2θ range = 10°–70° were typical measuring conditions. Profile fitting for the X-ray pattern was carried out using Pearson type VII as a profile shape function (3). In this procedure, we did not omit the $K\alpha_2$ peak numerically but a raw pattern was analyzed assuming the $K\alpha_1$ and $K\alpha_2$ peaks with an intensity ratio of 2:1, corresponding to one reflection. The excess oxygen contents of the samples were measured using a thermogravimetric analyzer (Perkin–Elmer TGA7). About 20 mg of powdered sample was placed in an alumina crucible and the weight loss was measured by increasing the temperature at a rate of 10 K/min under argon. A HRTEM study was carried out by using a microscope (Hitachi H-1500) operating at 800 kV. The magnetic susceptibility was measured under field-cooling and zero-field-cooling conditions at 10 G using a DC SQUID magnetometer (Quantum Design, MPMS). The electric resistivity measurements were carried out by a conventional DC four-probe method with silver as an electrode, using a physical property measurement system (Quantum Design, PPMS). Electron probe microanalysis (EPMA) was carried out for some selected samples to determine their metal contents using an analyzer (JEOL JXA-8600MX).

RESULTS AND DISCUSSION

For a nominal oxygen content of $x = 5.0$, the same tetragonal 1201 phase with lattice parameters, $a = 3.908(1)$ and $c = 8.101(3)$ Å, was obtained in both the quenching and slow-cooling procedures. Impurities of $SrCuO_2$, CuO, and other unknown oxide(s) were also found in the $x = 5.0$ samples in fairly large amounts. The 1201 phase purity increased substantially with the increase of the nominal oxygen content, and nearly single-phase samples were obtained in the range $5.2 \leq x \leq 5.5$. However, the phase purity decreases again for $x > 5.5$ (CuO was the major impurity in the latter samples).

Figure 1 shows X-ray diffraction patterns of the $x = 5.5$ samples. The quenched phase has a tetragonal lattice with $a = 3.920(1)$ and $c = 8.126(1)$ Å, while the slowly cooled sample has an orthorhombic lattice with $a = 3.934(1)$, $b = 3.875(1)$, and $c = 8.161(3)$ Å. In order to confirm the tetragonal symmetry in the quenched phase and the orthorhombic distortion in the slowly cooled phase, we carried out detailed step-scanning X-ray measurements and profile fitting of the patterns. Figure 2 shows the results of the fitting for the 2θ region between 62.4° and 64.6°. Only one 213 reflection (two peaks including the $K\alpha_2$ peak) or two reflections with 213 and 123 are expected in this region for the tetragonal and orthorhombic lattices, respectively. The pattern of the quenched phase was first analyzed assuming two reflections but they converged to a single reflection. On the other hand, two reflections were needed for successful fitting of the slowly cooled phase. A similar X-ray analysis was carried out for other samples with different oxygen contents. Quenched 1201 phases always have tetragonal lattices independently of the oxygen content, while slowly cooled phases have orthorhombic lattices, except for $x = 5.0$.

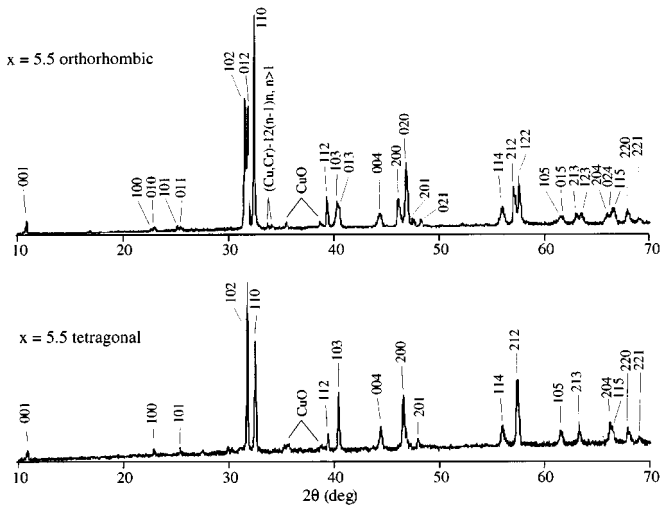

FIG. 1. Powder X-ray diffraction patterns for the $(Cu_{0.5}Cr_{0.5})Sr_2CuO_{5.5}$ samples obtained by the slow-cooling (orthorhombic, top) and quenching (tetragonal, bottom) procedures.

Figure 3 shows variations of the lattice parameters of the tetragonal and orthorhombic 1201 phases as a function of the oxygen content. For quenched tetragonal systems, the a parameter varies rather largely but is nearly independent of the oxygen content (taking an average value of $\approx$3.91 Å). For slowly cooled systems, the orthorhombic distortion is maximum at $x = 5.5$ and becomes smaller with an increase or decrease of the oxygen content, disappearing at $x = 5.0$.

Weight loss due to oxygen removal was observed by the TGA measurements. Figure 4 shows TGA curves of the quenched and slowly cooled samples with $x = 5.3$. Both curves have two plateaus around 500 and 700°C, and weight loss occurs in three steps. In the case of the quenched sample, the first weight loss of $\approx$0.45% is observed between $\approx$180 and $\approx$520°C, and this value indicates that $\approx$0.1 mole of oxygen per unit formula is removed. In the next step, between $\approx$520 and $\approx$720°C, further weight loss of

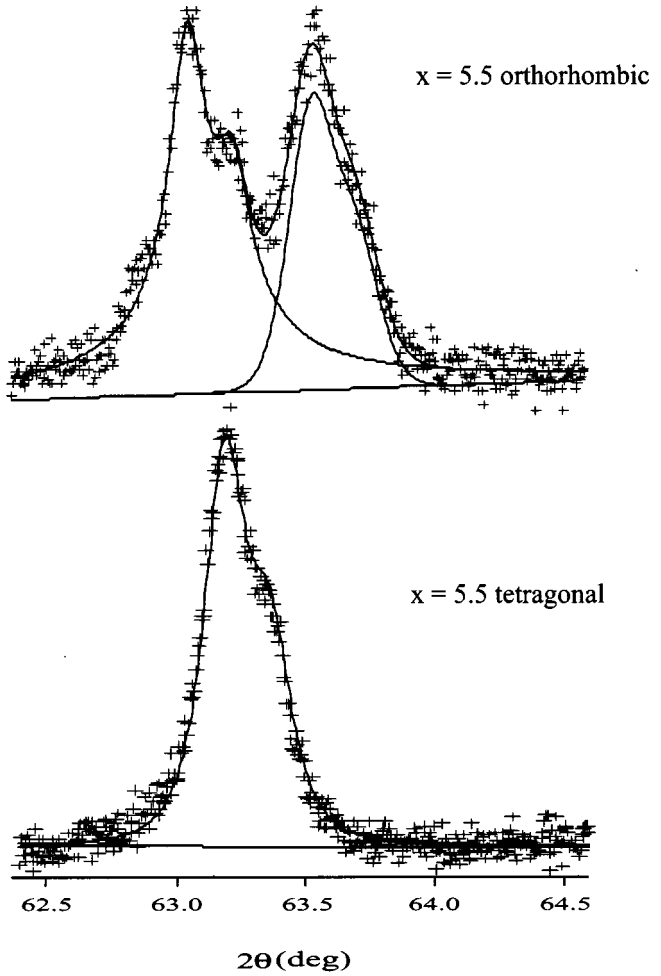

FIG. 2. X-ray profile fitting for the $(Cu_{0.5}Cr_{0.5})Sr_2CuO_{5.5}$ samples obtained by the slow-cooling (top) and quenching (bottom) procedures.

$\approx$0.9% is observed, which corresponds to the removal of $\approx$0.2 mole of oxygen. The final large weight loss starts at $\approx$720°C, and is probably associated with the decomposition of the 1201 phase. In the case of the slowly cooled sample, the first weight loss of $\approx$0.2% corresponds to $\approx$0.05 mole of oxygen and the second one of $\approx$1.1% to $\approx$0.25 mole. It should be noted that in both cases, total oxygen loss at the second plateau is close to 0.3 mole, which is the same value as the starting excess oxygen content (5.3–5.0). We obtained very similar results for the $x = 5.1$ and 5.2 samples and concluded that the second plateau corresponds to the state of $x = 5.0$ with the formal copper valence of $+2$, assuming an hexavalent oxidation state for chromium. For a sample with $x \geq 5.4$, the second and third steps of the weight losses tend to overlap, and the plateau around 700°C becomes less clear. However, the tetragonal and orthorhombic samples seemed to have nearly the same excess oxygen content as in the samples with $x \leq 5.3$. The first-step excess oxygen removal is less pronounced in the

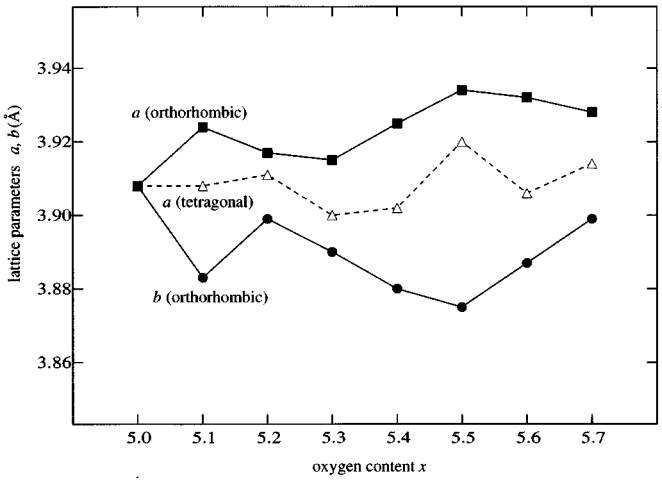

FIG. 3. Variation of a and b parameters of the tetragonal and orthorhombic 1201 phases as a function of the nominal oxygen content x.

$x = 5.3$ orthorhombic phase than in the tetragonal one. We suppose that this result reflects a more ordered and structurally bonded state of the excess oxygen atom in the orthorhombic phase.

The HRTEM observations showed that all tetragonal phases gave simple electron diffraction patterns consistent with the space group of $P4/mmm$, independently of the oxygen content. The electron diffraction spots were sharp without diffuse, and we did not find any evidence of a microdomain structure.

However, more complicated patterns were observed for the orthorhombic phases. Figure 5 shows $hk0$, $h0l$ and $0kl$ electron diffraction patterns of the $x = 5.5$ orthorhombic

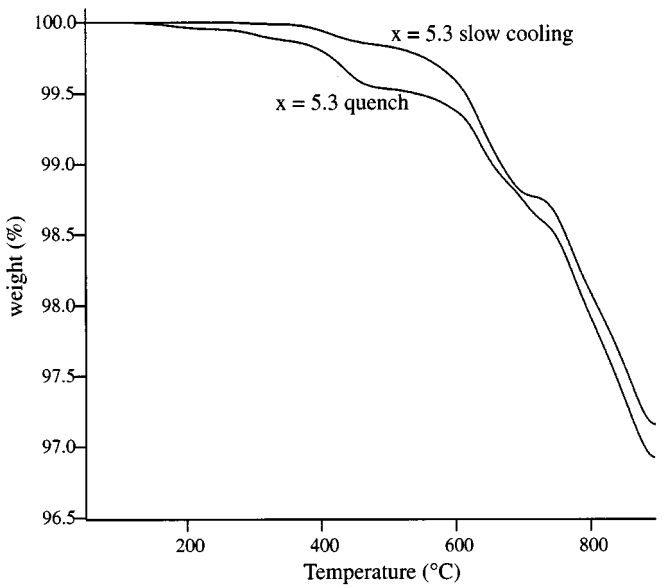

FIG. 4. TGA curves obtained under argon for the slowly cooled and quenched $(Cu_{0.5}Cr_{0.5})Sr_2CuO_{5.3}$ samples.

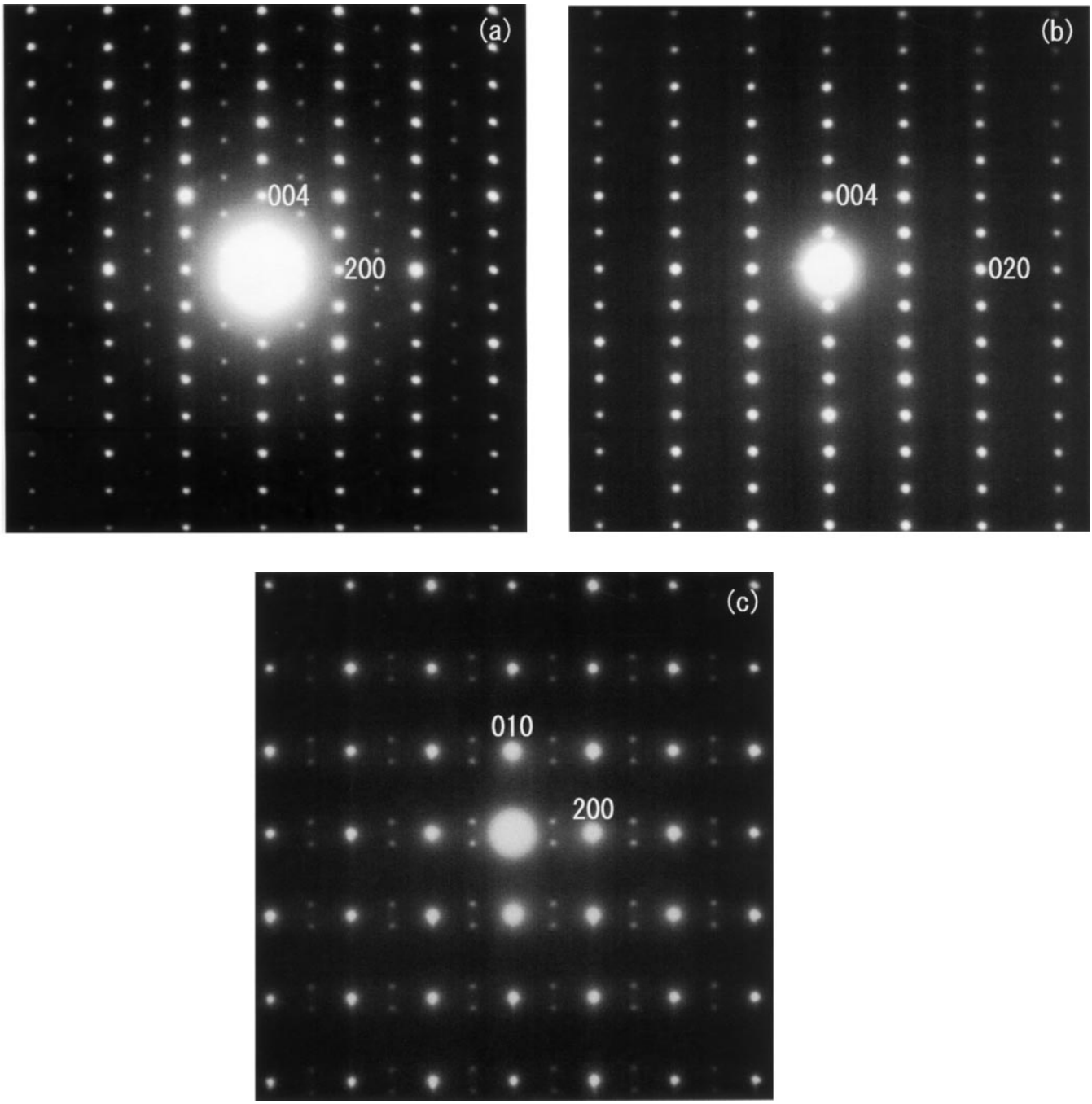

FIG. 5. The (a) *h*0*l*, (b) 0*kl*, and (c) *hk*0 electron diffraction patterns of the orthorhombic $(Cr_{0.5}Cu_{0.5})Sr_2CuO_{5.5}$ phase. Indexes are given based on the superlattice with $a_s = 2a$, $b_s = b$, $c_s = 2c$.

phase. Extra spots in the *h*0*l* section indicate a superlattice with double periodicity along the *a* and *c* axes, i.e., with $a_s = 2a$ and $c_s = 2c$, with respect to the simple orthorhombic lattice. No extra spots are present in the 0*kl* section, indicating $b_s = b$. The *hk*0 pattern is further complicated with the presence of weak incommensurate superspots whose origin is not known. The superlattice spots in the *h*0*l* section were observed in other orthorhombic phases with $x = 5.2$ and $x = 5.7$ but their relative intensities were much weaker when compared with the $x = 5.5$ phase. Figure 6 shows a lattice image of the orthorhombic phase projected along the *b* axis. The 1201-type stacking of planes along the *c* axis, $SrO–(Cu, Cr)O_{1+\delta}–SrO–CuO_2$, is seen clearly but the double periodicity along the *a* axis is not visible in the image.

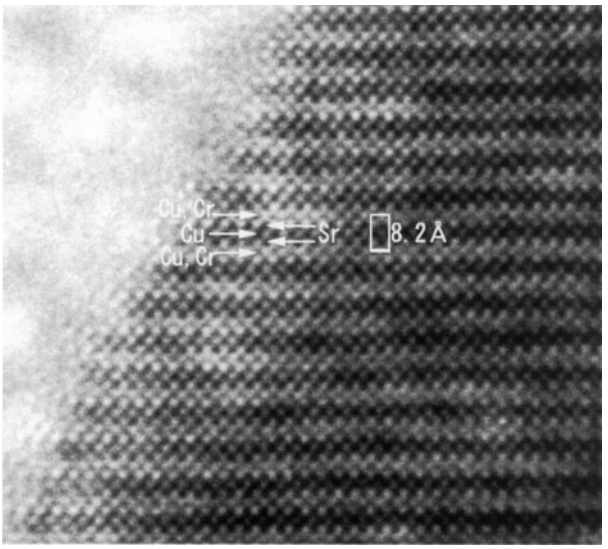

FIG. 6. HRTEM image projected along the *b* axis for the orthorhombic $(Cu_{0.5}Cr_{0.5})Sr_2CuO_{5.5}$ phase.

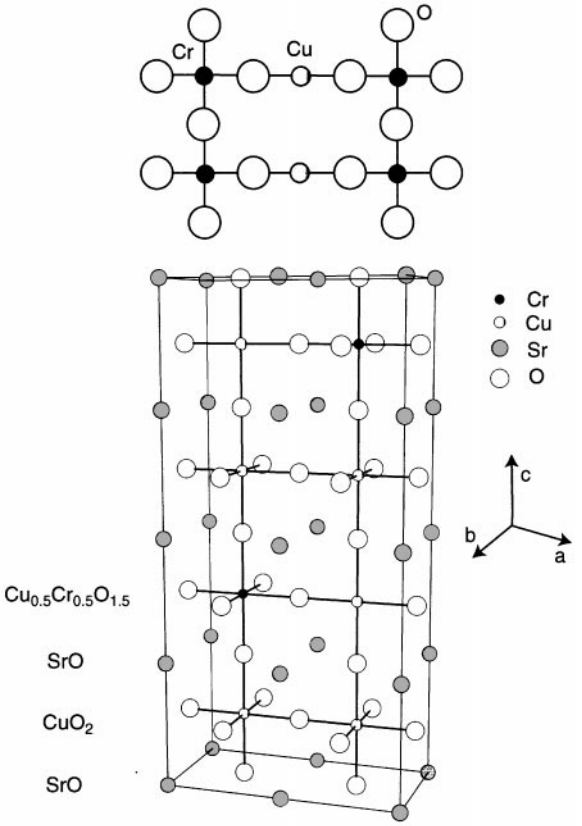

FIG. 7. Structure model for the orthorhombic $(Cu_{0.5}Cu_{0.5})Sr_2CuO_{5.5}$ phase.

Disregarding the incommensurate extra spots in the *hk*0 section, the electron diffraction patterns of the orthorhombic phase is consistent with the superlattice of $a_s = 2a$, $b_s = b$, $c_s = 2c$, and the possible space group of *Bmmm* (standard setting *Cmmm*). Similar superstructures have been reported for various $(Cu_{0.5}M_{0.5})A_2Ca_{n-1}Cu_nO_{2n+3}$ ((Cu, *M*)-12($n-1$)*n*, *A*: alkaline earth) series of phases where *M* is a nonmetal atom such as *M* = C (4, 5). S(6), or P(7). In these phases, copper and *M* are placed in an ordered way in the (Cu, *M*) plane as Cu–*M*–Cu–*M* $\cdots$ along the *a* axis, originating the double periodicity. The phase of the Cu–*M* sequence is different between adjacent (Cu, *M*) planes, resulting in the double periodicity along the *c* axis. When *M* is a metal atom such as Ge(8), Cr(1), or V(9), copper and *M* in the (Cu, *M*) plane are usually placed randomly and (Cu, *M*)-12($n-1$)*n* phases crystallize as simple tetragonal systems.

According to the aforementioned reports for the (Cu, *M*)-12($n-1$)*n* systems, we surmise that copper and chromium in the (Cu, Cr) are ordered as the Cu–Cr–Cu–Cr $\cdots$ plane in slowly cooled samples, whereas they are randomly distributed in quenched phases. The orthorhombicity and relative intensities of the *h*0*l* extra spots depend on the oxygen content. This results suggest strongly that the oxygen atom in the (Cu, Cr) plane has something to do with the ordering. In Fig. 7, a possible structure model is given for the orthorhombic phase. In this model, copper and chromium in the (Cu, Cr) plane are ordered as Cu–Cr–Cu–Cr $\cdots$. In addition, oxygen atoms are arranged so that copper is in square coplanar coordination and chromium in octahedral coordination. This structure includes 5.5 oxygen atoms per formula unit and seems to explain well the maximum orthorhombic distortion and the strongest *h*0*l* extra electron diffraction spots in the $x = 5.5$ phase. Neutron diffraction analysis is desired for the confirmation of the model. Moreover, further studies are needed to elucidate the modulated nature of the structure suggested by the *hk*0 electron diffraction pattern.

To see the metal contents of the present phases, EPMA measurements were carried out for the $x = 5.2$ and 5.4 samples. The results are shown in Table 1 where the Cr and Cu contents are calculated assuming a stoichiometric Sr content of 2. The Cr and Cu contents were almost independent of the oxygen content or the crystal system (orthorhombic or tetragonal). The Cr contents obtained are very close to 0.5, which is expected for the stoichiometric composition of $(Cu_{0.5}Cr_{0.5})Sr_2CuO_x$. However, the Cu contents are slightly smaller than 1.5 as pointed out previously (1). This result may suggest the presence of Cu vacancies and may be related to the incommensurate extra spots observed for the orthorhombic phase. We need further studies on this point.

The orthorhombic-to-tetragonal transition is well known for the $YBa_2Cu_3O_7$ phase to be induced when the oxygen atoms are removed from the CuO chain plane (10). This transition is related to the oxygen content of the system and

TABLE 1
EPMA Data for the (Cu, Cr)Sr_2CuO_x Phases[a]

x	Crystal system	Cr	Cu
5.2	Tetragonal	0.55(2)	1.25(4)
5.2	Orthorhombic	0.58(1)	1.30(3)
5.5	Tetragonal	0.55(1)	1.29(3)
5.5	Orthorhombic	0.51(2)	1.33(5)

[a]The Cr and Cu contents were calculated, assuming a stoichiometric Sr content of 2.

is, in a strict sense, an oxidation/reduction reaction rather than a structural transition. In contrast, we observed no significant difference in the excess oxygen contents of the orthorhombic and tetragonal (Cu, Cr)-1201 phases at least for $x \leq 5.3$. We concluded that the present phase undergoes orthorhombic-to-tetragonal transition due to order–disorder effects of the copper and chromium (and oxygen) atoms within the (Cu, Cr) plane when it is heated under high pressure.

The orthorhombic $YBa_2Cu_3O_7$ phase commonly has a twin defect structure that consists of two types of domains with different a axis (and b axis) orientations. The angle between the a axis of the two domains is near 90° and such twin structure can be well detected by the electron diffraction because each $hk0$ spot is split in two. For the present orthorhombic 1201 phase, we have never observed the splitting of the electron diffraction spots. The twin formation in $YBa_2Cu_3O_7$ is caused by the relatively low transition point (around 650°C in air (10)) between the tetragonal and orthorhombic forms. In such a low-temperature region, a domain cannot grow to form a grain with a single domain. According to this context, it is suggested that the present phase transition occurs in a high-temperature region where the system can get enough activation energy to make a single-domain grain.

Finally, we will briefly discuss the physical properties of the present system. Magnetic measurements carried out on all tetragonal phases showed the absence of superconductivity. However the orthorhombic phases with $x = 5.2$ and $x = 5.5$ showed weak diamagnetism (-7×10^{-4} and -7×10^{-5} emu/g at 5 K, respectively) below 35 and 20 K, respectively. Diamagnetism is absent in the orthorhombic samples with $x > 5.5$. In the X-ray patterns of the orthorhombic samples, unassigned extra peaks are often present around $2\theta = 34°$ (see Fig. 1). Although the present system does not include Ca, Sr-based members of the (Cu, Cr)$Sr_2Sr_{n-1}Cu_nO_{2n+3}$ homologous series with $n \geq 2$ can exist, and their strongest peaks are expected to appear in this 2θ region. We concluded that the 1201 system is not superconducting for the entire range of oxygen content, and that superconductivity observed in the slowly cooled samples is due to the presence of member(s) with $n \geq 2$ of the (Cu, Cr)$Sr_2Sr_{n-1}Cu_nO_{2n+3}$ homologous series included as impurities.

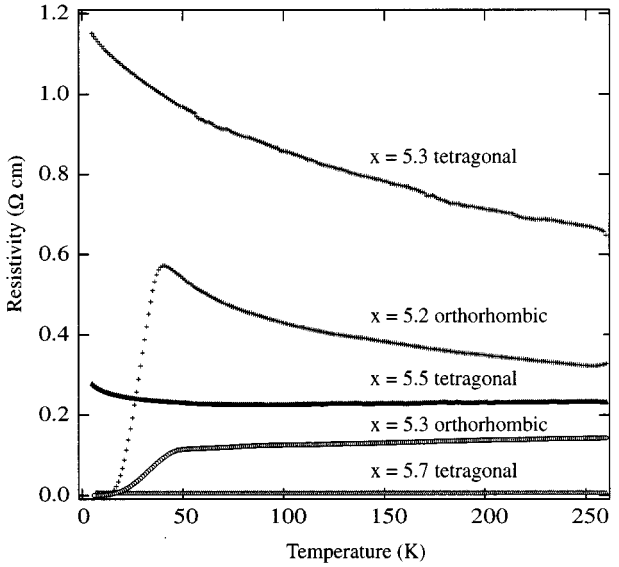

FIG. 8. Temperature dependence of electric resistivity for the orthorhombic and tetragonal $(Cu_{0.5}Cr_{0.5})Sr_2CuO_x$ phases with $x = 5.2$, 5.3, 5.5, and 5.7.

Figure 8 shows DC electric resistivity for selected orthorhombic and tetragonal samples. Comparing three tetragonal phases with $x = 5.3$, 5.5, 5.7, it is seen that the resistivity decreases drastically with increasing x (resistivity at 300 K is ≈ 0.9 Ωcm for $x = 5.2$ while $\approx 7 \times 10^{-3}$ Ωcm for $x = 5.7$). This systematic variation of the resistivity indicates that the oxygen content and carrier (hole) concentration in the 1201 phase actually increase when the starting oxygen content is increased. Superconducting transitions were observed in the $x = 5.2$ and $x = 5.3$ orthorhombic samples, consistent with the magnetic data. Although it appears that the $x = 5.3$ orthorhombic sample has a normal-state resistivity much smaller than that of the corresponding tetragonal one, the difference may be caused by the superconducting impurity phase(s) included in the orthorhombic sample.

In our previous report (1), we suggested that the overdoped state of carriers seemed to be the reason for the disappearance of superconductivity in the 1201 phase. However, the present study indicates that this is not the case. The electric resistivity of the 1201 phase is quite high even for $x = 5.7$, suggesting that carrier concentration is not high enough for inducing superconductivity even in the $x = 5.7$ phase, and that doped holes may be localized somewhere in the structure.

CONCLUSION

Several $(Cr_{0.5}Cu_{0.5})Sr_2CuO_x$ ((Cu, Cr)-1201) samples with varying oxygen content were prepared under high pressure and high temperature. They are tetragonal when

synthesized by a quenching procedure, and orthorhombic when slowly cooled, except for $x = 5.0$. The orthorhombic phase has a superstructure with $a_s = 2a$, $b_s = b$, $c_s = 2c$, relatively to the fundamental orthorhombic lattice. An ordered arrangement of Cu–Cr–Cu–Cr $\cdots$ along the a axis is proposed for the (Cu, Cr) plane of the orthorhombic phase. We concluded that the present system undergoes orthorhombic-to-tetragonal transition upon heating due to order–disorder effects within the (Cu, Cr) plane. Although the electric resistivity of the (Cu, Cr)-1201 system decreases drastically when the oxygen content is increased, bulk superconductivity is not observed for the entire range of oxygen doping.

ACKNOWLEDGMENTS

The author greatly acknowledges M. Akaishi and S. Yamaoka for their helpful suggestions on high-pressure synthesis. This work was supported by the Multi-Core Project and Special Coordination Funds of the Science and Technology Agency of the Japanese Government.

REFERENCES

1. S. M. Loureiro, Y. Matsui, and E. Takayama-Muromachi, *Physica C* **302,** 244 (1998).
2. M. Isobe, Y. Matsui, and E. Takayama-Muromachi, *Physica C* **273,** 72 (1996).
3. M. M. Hall Jr., V. G. Veeraraghavan, H. Rubin, and P. G. Winchell, *J. Appl. Crystallogr.* **10,** 66 (1977).
4. Y. Miyazaki, H. Yamane, N. Ohnishi, T. Kajitani, K. Hiraga, Y. Morii, S. Funahashi, and T. Hirai, *Physica C* **198,** 7 (1992).
5. T. Kawashima, Y. Matsui, and E. Takayama-Muromachi, *Physica C* **224,** 69 (1994).
6. E. Takayama-Muromachi, Y. Matsui, and J. Ramirez-Castellanos, *Physica C* **252,** 221 (1995).
7. M. Isobe, Y. Matsui, and E. Takayama-Muromachi, *Physica C* **273,** 72 (1996).
8. A. T. Matveev, J. Ramirez-Castellanos, Y. Matusi, and E. Takayama-Muromachi, *Physica C* **262,** 279 (1996).
9. N. D. Zhigadlo, Y. Anan, T. Asaka, Y. Ishida, Y. Matsui, and E. Takayama-Muromachi, *Chem. Mater.* **11,** 2185 (1999).
10. For instance, see following review and references therein, R. Beyers and T. M. Shaw, *in* "Solid State Physics" (H. Ehrenreich and D. Turnbull, Eds.), Vol. 42, p. 135. Academic Press, San Diego, 1989.